

Potential of Interaction between Nuclei and Nucleon-Density Distribution in Nuclei

V. Yu. Denisov* and V. A. Nesterov

Institute for Nuclear Research, National Academy of Sciences of Ukraine, pr. Nauki 47, 03680 Kiev, Ukraine

Received July 29, 2005; in final form, February 10, 2006

Abstract—Nuclear-interaction potentials that are calculated by using Skyrme forces within the extended Thomas–Fermi approximation and Hartree–Fock–Bardeen–Cooper–Schrieffer theory are studied in detail. It is shown that the nuclear component of the potential simulating the interaction between nuclei grows with increasing number of neutrons in colliding isotopes and with increasing diffuseness parameter of the density distribution in interacting nuclei. An increase in the diffuseness parameter of the density distribution in interacting nuclei leads to a decrease in the height of the barrier between the nuclei and to an increase in the depth of the capture well and in the fusion cross section. It is shown that the diffuseness parameter calculated for the nuclear component of the potential at large distance between interacting nuclei by using Skyrme forces exceeds the diffuseness parameter of the nucleon-density distribution in these nuclei by a factor of about 1.5. Realistic values of the diffuseness parameter of nuclear interaction between medium-mass and heavy nuclei fall within the range $a \approx 0.75\text{--}0.90$ fm.

PACS numbers : 21.10.Dr, 21.10.Ft, 21.10.Gv, 25.70.Jj

DOI: 10.1134/S1063778806090067

1. INTRODUCTION

In order to calculate various features of nuclear reactions, it is necessary to know the potential energy of interaction between the participant nuclei [1–3]. In view of this, the magnitude and the radial dependence of the nuclear-interaction potential at short distances between the nuclei are of paramount importance for describing cross sections for various reactions within any model.

The interaction energy of nuclei receives contributions from the Coulomb interaction of their protons and from the nuclear interaction of nucleons contained in them [1–3]. The Coulomb interaction of protons in colliding nuclei has been studied quite well, but the nuclear interaction of nuclei is known less precisely. In view of this, a rather large number of various approximations of nucleus–nucleus interaction have been proposed to date [1–8], these approximations leading to different heights of the barrier for nuclear fusion [8–11]. The barrier height is determined by the interplay of the Coulomb repulsion and nuclear-attraction potentials acting at short distances between the surfaces of interacting nuclei.

The relationship between the collision energy and the barrier height determines the nuclear-reaction mechanism. For example, an increase in the collision energy leads to an increase in the number of possible

reaction channels and to a change in the type of dominant channels. In nuclear-reaction theory, it is common practice to classify reactions on the basis of the relationship between the collision energy and the barrier height as subbarrier reactions, near-barrier reactions, threshold reactions, and so on. Since different approximations of the nucleus–nucleus component of the interaction lead to different values of the barrier height [1–9], the same reactions may have different mechanisms within different models. This point is of particular importance for describing the synthesis of superheavy nuclei. Such reactions are described within the models that were proposed in [9–17] and which are based on mutually exclusive concepts of the process of compound-nucleus formation. At the present time, it is therefore of paramount importance to know precisely the potential of interaction between participant nuclei and the respective barrier height.

In order to determine the nuclear interaction of nucleons that belong to different nuclei, it is desirable to apply the most precise methods that were developed for describing in detail various features of the ground states of the nuclei and their excited states [18–27]. By using these methods, one can also calculate the energy of the interaction of nuclei to a high precision. In this study, we will therefore employ the semiclassical and the semimicroscopic approach to determine the potential of the interaction of nuclei. Within the semiclassical approach, the nucleon-

*E-mail: denisov@kinr.kiev.ua

density distributions in interacting nuclei and the potential energy of their interaction are calculated in the extended Thomas–Fermi (ETF) approximation by using Skyrme forces. In the semimicroscopic approach, the nucleon-density distributions in interacting nuclei are determined in the Hartree–Fock–Bardeen–Cooper–Schrieffer (HF–BCS) approximation by using Skyrme forces, while the potential energy of their interaction is found in the ETF approximation implemented for the case of Skyrme forces. It should be noted that the ETF approximation and HF–BCS theory involving Skyrme forces describe well the binding energies of nuclei, the nucleon-density distributions in them, their root-mean-square radii, and many other features of the ground states of nuclei and their excited states [18–25, 27].

Subbarrier-fusion reactions [1–3, 28–36] are of importance from the point of view of determining the potential of nucleus–nucleus interaction, since such reactions are governed by the strength of the interaction and by the behavior of the potential at short distances between participant nuclei. A great many different models have been proposed to date for describing subbarrier-fusion reactions [1–3, 28–36]. Frequently, the parameters of nucleus–nucleus interaction are fitted in order to describe adequately the fusion cross section. By way of example, we indicate that, according to [32–36], an analysis of data on the subbarrier fusion of nuclei leads to quite large values of the diffuseness parameter of the nuclear component of the nucleus–nucleus potential parametrized in the form of the Woods–Saxon potential ($a \approx 0.8–1.5$ fm). At the same time, smaller values of the diffuseness parameter of the nuclear component of the nucleus–nucleus potential ($a \approx 0.6–0.7$ fm) are employed in many other studies [1–3, 7, 28–31] to describe various nuclear reactions.

In the double-folding approximation [2, 3, 8, 9], the diffuseness parameter of the potential can be related to the diffuseness of the nucleon-density distribution in nuclei and the effective range of nucleon–nucleon interaction. Since the effective range of nucleon–nucleon interaction is rather small [18], the diffusion parameter of the nucleon-density distribution is not expected to differ markedly from the diffuseness parameter of the nuclear component of the potential. Thus, it is of great interest to analyze comprehensively the diffuseness parameter of the nuclear component of the potential of nucleus–nucleus interaction within various models. It is also interesting to determine realistic values of the diffuseness parameter of the nuclear component of the nucleus–nucleus potential parametrized in the Woods–Saxon form.

This article is organized as follows. In Section 2, we describe briefly basic properties of the radial distribution of nucleon densities calculated for spherical

nuclei in various approximations. In Section 3, we calculate interaction potentials for various pairs of nuclei, employing the results obtained for the radial distributions of nucleon densities. Also, we discuss there in detail the barrier heights and the depths of the capture wells for various colliding systems. In Section 4, we analyze the potential of nucleus–nucleus interaction as a function of the diffuseness parameter of the nucleon-density distribution in the nuclei involved and discuss the relationships between the diffuseness parameter of the nucleon-density distribution, the diffuseness parameter of the nuclear component of the interaction potential, and the cross section for the fusion of nuclei. A brief summary is given in Section 5.

2. NUCLEON-DENSITY DISTRIBUTION IN NUCLEI

The radial distribution of nucleon densities in spherical nuclei was considered in various approximations [18–25, 27]. The ETF approximation implemented with Skyrme forces makes it possible to describe density distributions, binding energies, and other features of nuclei within the semiclassical approximation [18–23]. The quantum-mechanical self-consistent HF–BCS method employing Skyrme forces and taking into account pairing forces is yet another method for describing various properties of nuclei [18, 24, 25, 27]. The Hartree–Fock method describes nucleon-density distributions to a high precision and is a fully microscopic approach [18, 24, 27]. The self-consistent HF–BCS method was considered in detail in [18, 24]. A wide variety of properties of nuclei in their ground and excited states were described by using this method [18, 24, 25, 27]. The quantum-mechanical HF–BCS method is quite involved, while the ETF approximation is simple and clear. Below, we will briefly consider the application of the ETF approximation to describing nucleon-density distributions in nuclei and compare the results obtained in this way with the predictions of the HF–BCS method.

2.1. Modified Thomas–Fermi Approximation

The ETF method is specified by the equations [18, 19, 22, 23]

$$\frac{\delta\mathcal{E}(\rho_n, \rho_p)}{\delta\rho_p} - \lambda_p = 0, \quad (1)$$

$$\frac{\delta\mathcal{E}(\rho_n, \rho_p)}{\delta\rho_n} - \lambda_n = 0, \quad (2)$$

which are obtained from the variational principle where the total energy of the nucleus is treated as a functional of the neutron and proton densities (ρ_n

and ρ_p , respectively). The total energy of the nucleus, $E(\rho_n, \rho_p)$, is obviously expressed in terms of the respective energy density $\mathcal{E}(\rho_n, \rho_p)$ and is given by

$$E(\rho_n, \rho_p) = \int d\mathbf{r} \mathcal{E}(\rho_n, \rho_p) \quad (3)$$

$$= \int d\mathbf{r} (\tau + \varepsilon_{\text{pot}} + \varepsilon_{\text{Coul}}),$$

where τ , ε_{pot} , and $\varepsilon_{\text{Coul}}$ are the densities of, respectively, the kinetic, the potential nuclear, and the Coulomb energy and $\tau = \tau_n + \tau_p$ is the sum of the densities of the proton and neutron kinetic energies. We note that the nucleon matter densities and kinetic-energy densities depend on the spatial coordinates \mathbf{r} , but this dependence is omitted in Eqs. (1)–(3) and below in order to avoid encumbering the notation. In Eqs. (1) and (2), λ_n and λ_p are Lagrange multipliers that are the chemical potentials for, respectively, neutrons and protons and which are associated with the requirement that the number of neutrons, N , and the number of protons, Z , in the nucleus be conserved:

$$\int d\mathbf{r} \rho_{n(p)}(\mathbf{r}) = N(Z). \quad (4)$$

Within the ETF approximation, the kinetic energy density to second-order terms in \hbar is [19, 22]

$$\tau_{n(p)} = \tau_{\text{TF},n(p)} + \tau_{2,n(p)}, \quad (5)$$

where

$$\tau_{\text{TF},n(p)} = k\rho_{n(p)}^{5/3} \quad (6)$$

is the density of the neutron (proton) kinetic energy in the Thomas–Fermi approximation, with $k = \frac{5}{3}(3\pi^2)^{2/3}$, and $\tau_{2,n(p)}$ is the second-order gradient correction in \hbar . With allowance for all possible terms, this correction has the form [19, 22]

$$\tau_{2q} = b_1 \frac{(\nabla \rho_q)^2}{\rho_q} + b_2 \nabla^2 \rho_q + b_3 \frac{(\nabla f_q \nabla \rho_q)}{f_q} \quad (7)$$

$$+ b_4 \rho_q \frac{\nabla^2 f_q}{f_q} + b_5 \rho_q \left(\frac{\nabla f_q}{f_q} \right)^2 + b_6 h_m^2 \rho_q \left(\frac{\mathbf{W}_q}{f_q} \right)^2,$$

where the coefficients take the values of $b_1 = 1/36$, $b_2 = 1/3$, $b_3 = 1/6$, $b_4 = 1/6$, $b_5 = -1/12$, and $b_6 = 1/2$ and where we have used the following notation: $h_m = \hbar^2/(2m)$, $f_{n(p)} = 1 + \hbar_m(\alpha + \beta)\rho_{n(p)} + \hbar_m\alpha\rho_{p(n)}$, $\alpha = (1/4)[t_1(1 + x_1/2) + t_2(1 + x_2/2)]$, and $\beta = (1/4)[t_1(x_1 + 1/2) + t_2(x_2 + 1/2)]$. Hereafter, t_0 , t_1 , t_2 , t_3 , x_0 , x_1 , x_2 , x_3 , and α are the parameters of the Skyrme potential [18, 19, 24, 25], while $q = n$ or p . We note that the last term in (7) stems from taking into account spin–orbit

interaction. In the second order in \hbar with respect to the kinetic energy, we have

$$\mathbf{W}_{n(p)} = \frac{W_0}{2} [2\nabla \rho_{n(p)} + \nabla \rho_{p(n)}],$$

where W_0 is the strength parameter of spin–orbit interaction for the Skyrme potential (see [18, 19, 24, 25]).

In the case of Skyrme forces considered in [18, 19, 22–25], the potential-energy density is given by

$$\varepsilon_{\text{pot}} = \frac{1}{2} t_0 \left[\left(1 + \frac{1}{2} x_0 \right) \rho^2 - \left(x_0 + \frac{1}{2} \right) (\rho_n^2 + \rho_p^2) \right] + \frac{1}{12} t_3 \rho^{\alpha} \quad (8)$$

$$\times \left[\left(1 + \frac{1}{2} x_3 \right) \rho^2 - \left(x_3 + \frac{1}{2} \right) (\rho_n^2 + \rho_p^2) \right]$$

$$+ \frac{1}{4} \left[t_1 \left(1 + \frac{1}{2} x_1 \right) + t_2 \left(1 + \frac{1}{2} x_2 \right) \right] \tau \rho$$

$$+ \frac{1}{4} \left[t_2 \left(x_2 + \frac{1}{2} \right) - t_1 \left(x_1 + \frac{1}{2} \right) \right] (\tau_n \rho_n + \tau_p \rho_p)$$

$$+ \frac{1}{16} \left[3t_1 \left(1 + \frac{1}{2} x_1 \right) - t_2 \left(1 + \frac{1}{2} x_2 \right) \right] (\nabla \rho)^2$$

$$- \frac{1}{16} \left[3t_1 \left(x_1 + \frac{1}{2} \right) + t_2 \left(x_2 + \frac{1}{2} \right) \right]$$

$$\times ((\nabla \rho_p)^2 + (\nabla \rho_n)^2) + \frac{1}{2} W_0 [(\mathbf{J}_n + \mathbf{J}_p) \nabla \rho$$

$$+ \mathbf{J}_n \nabla \rho_n + \mathbf{J}_p \nabla \rho_p],$$

where $\rho = \rho_n + \rho_p$ and

$$\mathbf{J}_{n(p)} = -\frac{h_m}{f_{n(p)}} \rho_{n(p)} \mathbf{W}_{n(p)}.$$

Upon taking into account the exchange term in the Slater approximation, the Coulomb energy density assumes the form

$$\varepsilon_{\text{Coul}}(\mathbf{r}) = \frac{1}{2} e^2 \rho_p(\mathbf{r}) \int d\mathbf{r}' \frac{\rho_p(\mathbf{r}')}{|\mathbf{r} - \mathbf{r}'|} \quad (9)$$

$$- \frac{3}{4} e^2 \left(\frac{3}{\pi} \right)^{1/3} \rho_p^{4/3}(\mathbf{r}),$$

where e is the proton charge.

In the spherically symmetric case, Eqs. (1) and (2) reduce to the set of nonlinear integro-differential equations that was obtained in [22] and which is solved numerically by the method of successive approximations, the boundary conditions for these equations requiring that

$$\rho_q(r)|_{r \rightarrow \infty} = r^{-2} \exp \left(-\sqrt{|\lambda_q|/(h_m b_1)} r \right) \quad (10)$$

and that $\rho_q(r)$ be finite for $r \rightarrow 0$. By numerically solving these equations, one can find the radial distributions of neutron and proton densities in nuclei in the ETF approximation (for more details, see [22, 23]).

2.2. Results of the Calculation of Nucleon-Density Distributions in Nuclei

The radial distributions of the proton and neutron densities in the ground states of the ^{208}Pb and ^{48}Ca nuclei are given in Fig. 1 according to calculations performed in the ETF approximation by using the *SkP* [25] set of parameters for Skyrme forces. These density distributions are contrasted against their counterparts calculated in the self-consistent HF–BCS approximation with the same set of parameters of Skyrme forces and against the experimental charge-density distributions obtained from an analysis of data on electron scattering by these nuclei [37].

The proton densities calculated in the ETF approximation are in satisfactory agreement with their experimental counterparts and with those that were calculated in the HF–BCS approximation. However, the densities found in the semiclassical approximation decrease faster in the diffuse region and at long distances than the experimental densities and the densities calculated in the HF–BCS approximation. Therefore, the value found for the diffuseness parameter of the density distribution in the ETF approximation is somewhat smaller than that which was extracted from experimental data and than that which was calculated in the quantum-mechanical HF–BCS approximation.

In the region of the diffuse boundary of nuclei, the radial density distributions calculated in the HF–BCS approximation agree well with those extracted from data (see Fig. 1). In the interior of nuclei, however, the quantum-mechanical density distributions feature fluctuations whose amplitude is much greater than the amplitude of respective fluctuations in the experimental charge densities.

The distinctions between the density distributions found in the semiclassical and in the quantum-mechanical approach stem not only from the disregard of shell effects in the semiclassical approach but also from the distinctions between the values of the constant b_1 in expression (7) for the kinetic energy: 1/36 in the semiclassical case versus the quantum-mechanical value of 1/4 [19, 20]. This also leads to the difference in the asymptotic behavior of the densities, which is determined by expression (10). As a result, the densities obtained in the semiclassical approximation decrease at the boundary of a nucleus much faster than the densities found within the quantum-mechanical HF–BCS method (see Fig. 1).

3. POTENTIAL ENERGY OF INTERACTION BETWEEN NUCLEI

In the frozen-density approximation, the potential energy of interaction between two nuclei separated by a distance R , $V(R)$, will be defined here as the difference of the binding energies of the system of these two nuclei at a finite and at an infinite distance between them [8, 9, 38],

$$V(R) = E_{12}(R) - (E_1 + E_2). \tag{11}$$

The corresponding binding energies of the nuclear system in question and of nuclei 1 and 2 can readily be found by substituting the known nucleon-density distributions in the nuclei into the semiclassical expressions for the energy-density functional:

$$E_{12} = \int \varepsilon[\rho_{1p}(\mathbf{r}) + \rho_{2p}(\mathbf{r}, R), \rho_{1n}(\mathbf{r}) + \rho_{2n}(\mathbf{r}, R)]d\mathbf{r}, \tag{12}$$

$$E_1 = \int \varepsilon[\rho_{1p}(\mathbf{r}), \rho_{1n}(\mathbf{r})]d\mathbf{r}, \tag{13}$$

$$E_2 = \int \varepsilon[\rho_{2p}(\mathbf{r}), \rho_{2n}(\mathbf{r})]d\mathbf{r}. \tag{14}$$

The nucleus–nucleus potential at finite distances between the surfaces of nuclei owes its existence to the interaction of nucleons in the region of the overlapping tails of the nucleon-density distributions. Therefore, the inclusion of the gradient terms in the kinetic-energy density (7) is of importance for accurately calculating the potential.

In a collision of two nuclei, each of them affects the nucleon distribution in its collision partner owing to the effect of both the Coulomb and the nuclear component of the nucleon–nucleon interaction. In the frozen-density approximation, it is assumed that the interaction of nuclei does not change nucleon densities. Obviously, this approximation is valid at the initial stage of a collision process, as long as the nuclear densities overlap only slightly, so that the interaction of nucleons belonging to different colliding nuclei is weak. In collisions of heavy nuclei at near-barrier energies, the density distributions in colliding nuclei do not have time to change sizably at the initial stage of the collision process either. The time t_s over which nuclei traverse the strong-interaction region of size $s \approx 3$ fm can be estimated as

$$t_s \approx R_t[2\mu s/(e^2 Z_1 Z_2)]^{1/2},$$

where R_t is the distance equal to the sum of the radii of the nuclei, μ is their reduced mass, and Z_1 and Z_2 are the numbers of protons in the interacting nuclei. As a rule, $t_s \leq 10^{-21}$ s in collisions of heavy nuclei. The relaxation time for internal nuclear states that is associated with nucleon–nucleon interaction can

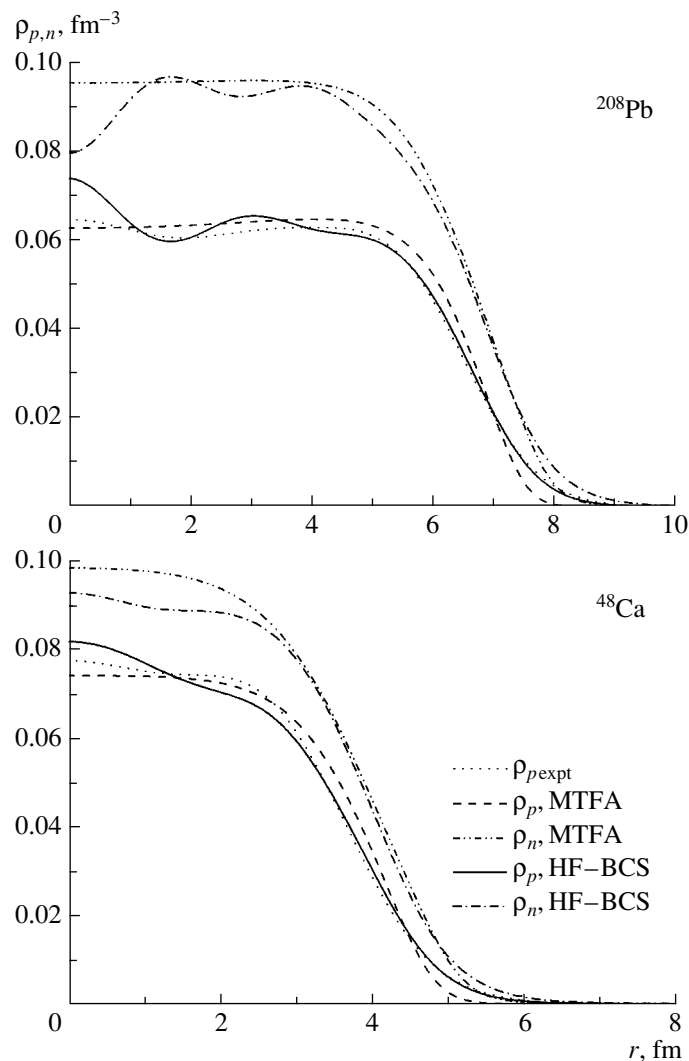


Fig. 1. Radial distributions of the proton and neutron densities in ^{48}Ca and ^{208}Pb nuclei according to calculations in the extended Thomas–Fermi approximation (ETFA) and within Hartree–Fock–Bardeen–Cooper–Schrieffer (HF–BCS) theory. For the sake of comparison, the calculated proton densities are plotted along with the respective charge densities extracted from experimental data on electron scattering by ^{48}Ca and ^{208}Pb nuclei.

be estimated as $t_{\text{relax}} \approx 2 \times 10^{-22} / \varepsilon^*$ s [9, 39], where ε^* is the excitation energy in megaelectronvolts per nucleon in the nuclear system being considered. At near-barrier energies of a collision between two rather heavy nuclei, ε^* is below $5/A$ MeV, where A is the number of nucleons in the system; therefore, $t_{\text{relax}} \approx 0.4A \times 10^{-22}$ s. It follows that, for heavy systems containing about 50 or more nucleons, the relaxation time is longer than the time over which such a nucleus traverses the strong-interaction region. In this case, the nucleon-density distributions do not have time to change sizably as the nuclei involved traverse the strong-interaction region; as a result, the frozen-density approximation is valid. Since t_{relax} grows with increasing A , this approximation becomes more justified for heavier systems.

The nucleus–nucleus potentials $V(R)$ for the $^{16}\text{O} + ^{16}\text{O}$, $^{66}\text{Zn} + ^{66}\text{Zn}$, $^{118}\text{Sn} + ^{118}\text{Sn}$, and $^{208}\text{Pb} + ^{208}\text{Pb}$ combinations are displayed in Fig. 2 according to calculations in the ETF approximation. The depth of the capture well is seen (Fig. 2) to decrease substantially with increasing mass number of interacting nuclei. Moreover, there is no capture well in the $^{208}\text{Pb} + ^{208}\text{Pb}$ system at all. The absence of the capture well or a decrease in its depth and width in heavy systems is explained by a considerable increase in the Coulomb energy of the repulsion of nuclei with increasing number of nucleons in them, this increase not being compensated by the corresponding increase in the attraction of these nuclei.

As the mass number increases, the capture well is shifted toward larger distances, the minimum of

the capture well occurring at a distance exceeding the sum of the root-mean-square radii of interacting nuclei for medium-mass and heavy systems or a distance smaller than the analogous sum for light systems (see Fig. 2).

In the frozen-density approximation, the potential energy of the interaction between colliding nuclei increases sharply at distances smaller than the sum of the radii of the nuclear surfaces because of a strong nuclear repulsion. This repulsion is due to the compressibility of nuclear matter and to a strong overlap of the densities of interacting nuclei, this leading to the emergence of the region where the density of nuclear matter exceeds a normal nuclear density. A sharp growth of the potential energy because of a strong overlap of the densities also leads to the relaxation of the density. We note that, as the nucleon excitation energy ε^* in the nuclear system grows, the relaxation time decreases, with the result that the nucleon-density distribution begins to change, whence it follows that the frozen-density approximation becomes invalid. Thus, it is legitimate to apply the frozen-density approximation to analyzing nucleus–nucleus potentials $V(R)$ only in the vicinity of the barrier and in the vicinity of the point at which interacting nuclei touch each other. Respective information about the potential $V(R)$ is of use for describing various near-barrier nuclear reactions. At smaller distances between nuclei, the frozen-density approximation may be valid only at high collision energies.

The capture well plays an important role in a collision of two heavy nuclei. Participant nuclei overcome the barrier within a rather short time and reach the capture well at the initial stage of the collision process. Various states of the system of two strongly overlapping nuclei are populated in the capture well, where there occur various processes characterized by the number of open reaction channels and by the probabilities of transitions between these channels. Some of these channels produce a complex excited system of strongly overlapping nuclei, while the others lead to the separation of nuclei. A complex excited state of strongly overlapping nuclei that arises in the capture well forms the entrance channel for the production of a compound nucleus or for the fusion–fission reaction. States that are formed in the capture well and which are associated with outgoing nuclei contribute to the elastic channel and to various inelastic reaction channels. It follows that, in the case of heavy systems, the absence of a capture well leads to a change in the reaction mechanism and hinders the formation of a compound nucleus. Nucleon–nucleon collisions in the capture well also lead to the relaxation of the nuclear density, with the result that the nucleon-density distribution changes smoothly

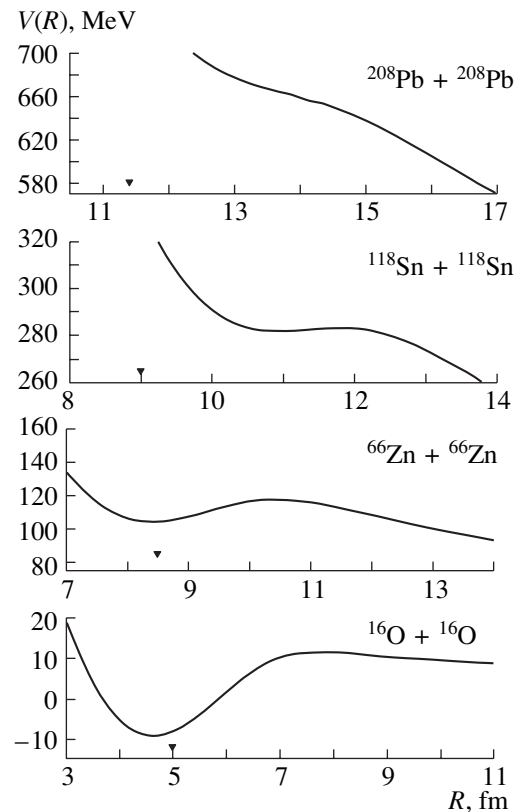


Fig. 2. Interaction potential for the $^{16}\text{O} + ^{16}\text{O}$, $^{66}\text{Zn} + ^{66}\text{Zn}$, $^{118}\text{Sn} + ^{118}\text{Sn}$, and $^{208}\text{Pb} + ^{208}\text{Pb}$ pairs of colliding nuclei according to calculations in the extended Thomas–Fermi approximation. Points (▼) indicate the position of the sum of the root-mean-square radii of colliding nuclei.

from a frozen to an adiabatic one. The potential of nucleus–nucleus interaction also undergoes changes owing to this relaxation of the nucleon density.

The potential $V(R)$ of the interaction between ^{64}Ni and the nuclei of five tin isotopes $^{100,114,118,124,132}\text{Sn}$ are displayed in Fig. 3 according to calculations in the ETF approximation. Also given in this figure are the proton and neutron densities for these isotopes. As the mass number of tin isotopes increases, the neutron-density distribution becomes more extended, but this concerns the proton densities to a smaller extent. This leads to the formation of a neutron skin in tin isotopes featuring a high neutron excess. The above properties of the neutron and proton densities lead to a strong isotopic dependence of the potential of interaction between respective nuclei. By way of example, we indicate that, with increasing mass number of tin isotopes, the barrier height decreases, while the depth and the width of the capture well increase. The isotopic dependence of the barrier height and of the potential is also confirmed by experimental data. According to the measurements

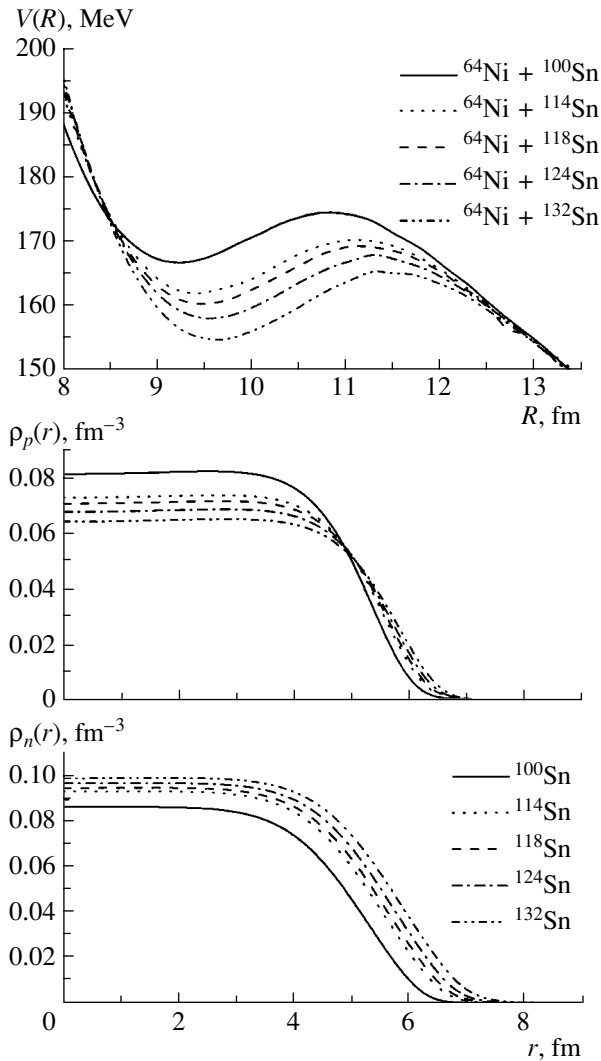


Fig. 3. Potentials of interaction between ^{64}Ni and nuclei of the tin isotopes $^{100,114,118,124,132}\text{Sn}$ along with the radial distributions of the proton and neutron densities in these isotopes according to calculations in the ETF approximation.

reported in [40], the fusion cross sections at barrier energies for reactions involving neutron-rich nuclei ^{132}Sn are larger than the analogous cross sections for reactions involving other tin isotopes that lie along the beta-stability line.

As was mentioned above (see also Fig. 1), the nucleon-density distributions calculated according to HF-BCS theory have a larger thickness of the diffuseness layer than those that were found in the ETF approximation. In view of this, it is reasonable to compare potentials obtained within the different approximations. Figure 4 shows the interaction potentials calculated for the system of ^{48}Ca and ^{208}Pb nuclei in the ETF approximation and in HF-BCS theory.

The potential obtained in the HF-BCS approximation has a lower barrier height and a narrower capture well than the potential found in the semiclassical approximation (see Fig. 4). This is because the nucleon-density distributions calculated in the HF-BCS approximation are characterized by a thicker diffuseness layer of a nucleus in relation to those that were found in the semiclassical approximation. Because of these properties of the nucleon-density distributions, the nuclear interaction between nuclei at long distances between their surfaces is stronger in the HF-BCS approximation than in the ETF approximation, while the Coulomb interaction is nearly identical in these two cases. The growth of the nuclear component of the interaction between nuclei at long distances between their surfaces reduces the height of the barrier between these nuclei. Owing to a greater diffuseness of the nucleon density, the region of a strong overlap of the densities belonging to the different nuclei becomes narrower, which leads to a reduction of the nuclear repulsion at short distances between interacting nuclei. As a result, the width and the depth of the capture well increase. This highlights a strong effect of the diffuseness of the nuclear-matter-density distribution on the properties of the potential of nucleus-nucleus interaction.

The interaction potentials calculated on the basis of the simple expressions proposed in [1, 4–8] are presented in Fig. 4 for the sake of comparison. The potentials proposed in [5, 6] are defined only to the point at which the nuclei involved touch each other; therefore, they are given in Fig. 4 only to this point as well, which corresponds to $R_t \approx 11.5$ fm. In particular, Fig. 4 shows the results obtained by using the potential parametrizations proposed by Bass in 1974 and 1980 [1] (Bass 1974 and Bass 1980 in the figure). We can see that the potentials calculated in the different approximations differ substantially from one another in the barrier region. The different parametrizations yield different barrier heights, this leading to ambiguities in describing fusion and fusion-fission reactions, as well as reactions involving the synthesis of superheavy nuclei. We note that the half-width of the maximum of the cross section for the formation of a heavy nucleus is about 3 MeV [41], which is much less than the uncertainty in the barrier due to the use of the various theoretical approximations for the nucleus-nucleus interaction.

The behavior of the potentials found in the different approximations is also markedly different at distances shorter than $R_t \approx 11.5$ fm (see Fig. 4). Therefore, the assumptions that can be inferred from an analysis of these potentials at short distances for the mechanisms that would govern nuclear reactions after the nuclei overcome the barrier may also be markedly different.

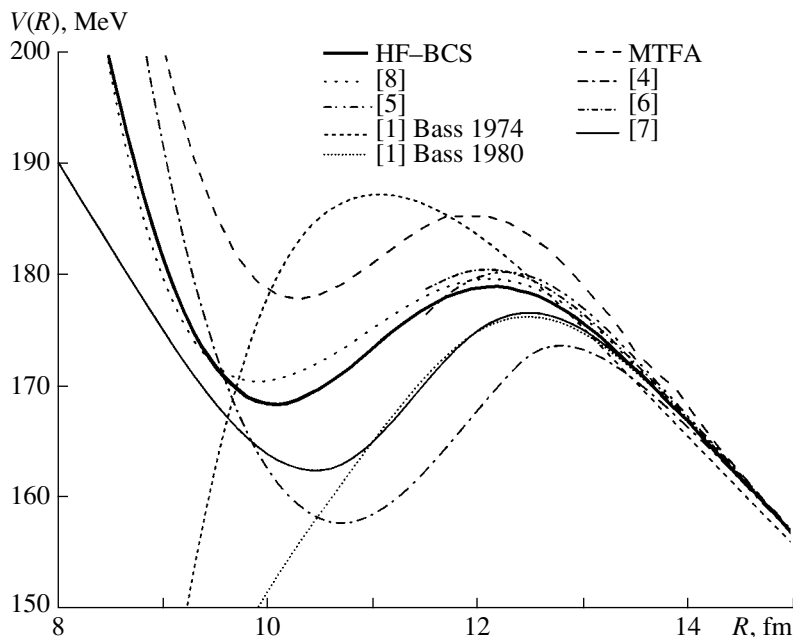


Fig. 4. Potentials of interaction between the ^{48}Ca and ^{208}Pb nuclei according to calculations performed in the extended Thomas–Fermi approximation (ETFA) and within Hartree–Fock–Bardeen–Cooper–Schrieffer (HF–BCS) theory by using Skyrme forces, along with the results obtained by calculating these potentials on the basis of the expressions proposed in [1, 4–8].

4. DIFFUSENESS OF THE DENSITY DISTRIBUTIONS AND DIFFUSENESS OF THE NUCLEAR COMPONENT OF THE NUCLEUS–NUCLEUS INTERACTION

4.1. Diffuseness of Nucleon Densities and Properties of the Nucleus–Nucleus Interaction Potential

In order to study in greater detail the effect of the diffuseness of the nucleon densities in colliding ground-state nuclei on the nucleus–nucleus potential, we parametrize such nucleon densities in the form

$$\rho_{n(p)} = \rho_{0n(p)} / \{1 + \exp[(r - R_{n(p)})/d]\}. \quad (15)$$

This parametrization of radial nucleon-density distributions is frequently used in nuclear physics [42]. The parameters $\rho_{0n(p)}$ and $R_{n(p)}$ of such distributions were found by the direct variational method at a fixed value of the diffuseness parameter d of the density distributions. By varying $\rho_{0n(p)}$ and $R_{n(p)}$, we minimized the binding energy calculated for the nucleus being considered with allowance for the gradient corrections in the kinetic-energy functional for the case of SkP Skyrme forces. The diffuseness parameter d of the neutron and proton densities was varied with a step of 0.05 fm over the interval between 0.5 and 0.8 fm. The radial distributions of the neutron and proton densities in the ground states of the ^{16}O and ^{208}Pb nuclei are given in Fig. 5 for the above values of

the diffuseness parameter. These densities were used to calculate the potentials of nucleus–nucleus interaction, which are also displayed in Fig. 5. In order to calculate the potential, we employed the ETF approximation and assumed the case of SkP Skyrme forces. Also presented in Fig. 5 for the sake of comparison is the potential of the interaction between the ^{16}O and ^{208}Pb nuclei according to the calculation within HF–BCS theory for the same parametrization of Skyrme forces.

At large distances between the nuclei, the potential calculated in the HF–BCS approximation is close to the potential based on the parametrization of the density in the form (15) at a diffuseness-parameter value in the range $d \approx 0.50\text{--}0.55$, but, at shorter distances, it is close to the potential calculated at $d \approx 0.60$ fm (see Fig. 5).

As the diffuseness parameter d of the density distribution grows, the capture well is shifted toward larger distances between colliding nuclei. Concurrently, the well becomes deeper, while the potential-barrier height decreases. The reason is that, with increasing diffuseness of the density distribution, the nucleon densities become more extended; as a result, the nuclear interaction at large distance between the nuclei involved grows, which leads to the reduction of the barrier height. With increasing diffuseness d of the density distributions, the nuclear densities begin to overlap strongly at smaller distances between

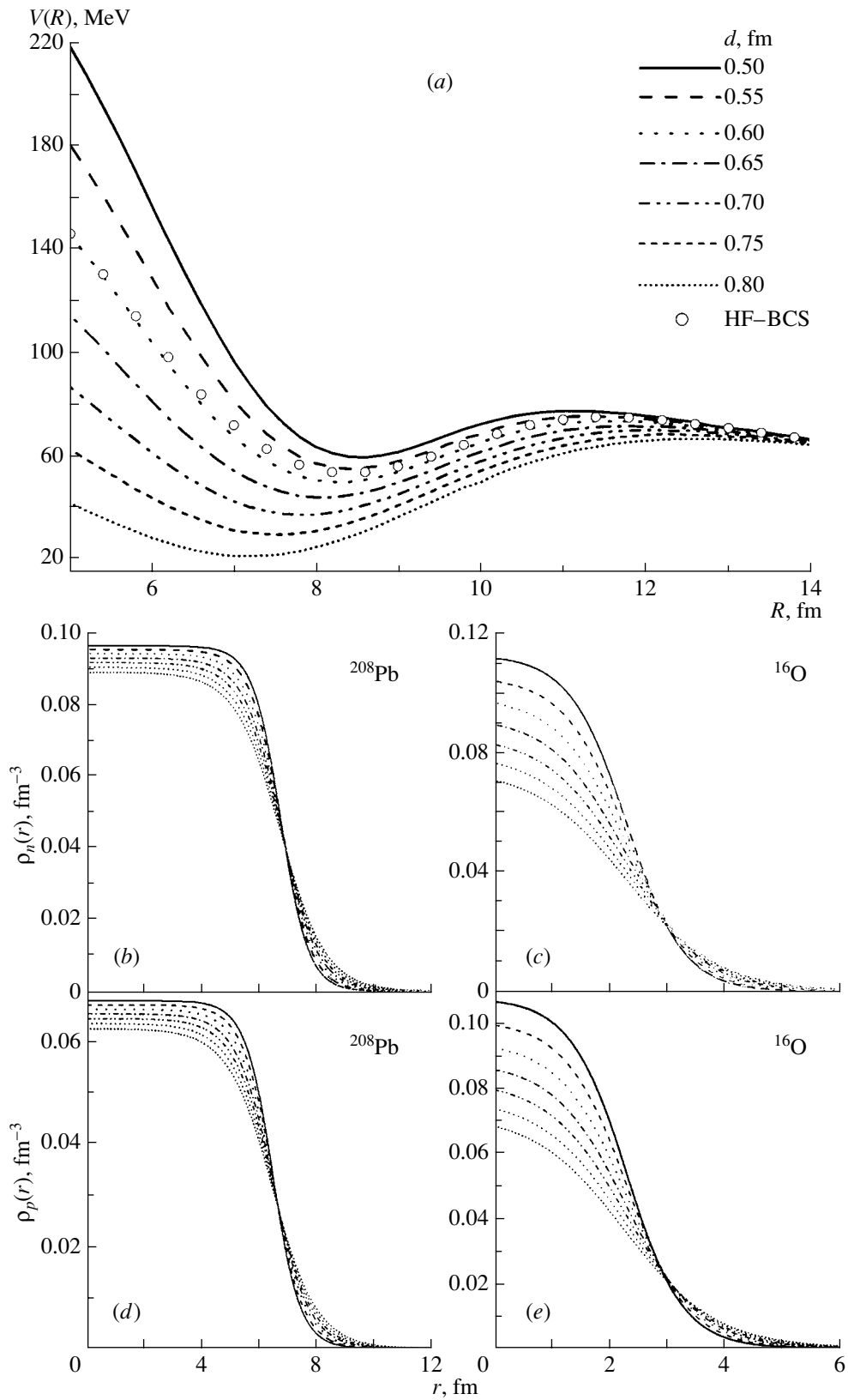


Fig. 5. (a) Interaction potentials calculated for pairs of ^{16}O and ^{208}Pb nuclei in the semiclassical approximation at various values of the diffuseness parameter d of the ground-state densities (curves). Also given for the sake of comparison the potential found in the Hartree–Fock–Bardeen–Cooper–Schrieffer (HF–BCS) approximation by using Skyrme forces (open circles). (b, c, d, e) Proton and neutron densities in the ground states of the ^{16}O and ^{208}Pb nuclei at various values of the diffuseness parameter d .

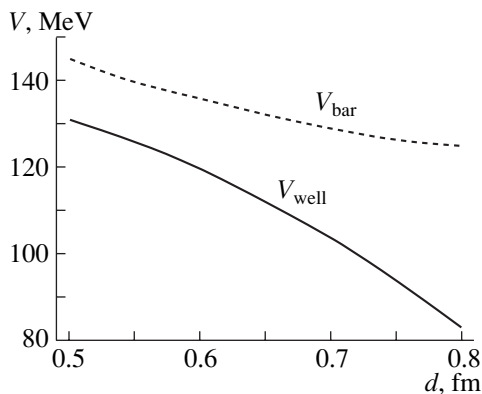


Fig. 6. Potential-barrier height $V_{\text{bar}}(d)$ and potential value at the bottom of the capture well, $V_{\text{well}}(d)$, versus the diffuseness parameter d of the ground-state nucleon densities for the $^{16}\text{O} + ^{208}\text{Pb}$ system.

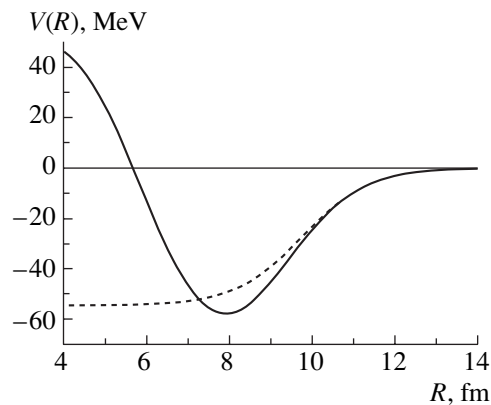


Fig. 8. Approximation of the interaction potential for the ^{16}O and ^{208}Pb nuclei that was obtained in the ETF approximation (solid curve) by a potential of the Woods–Saxon form (dashed curve).

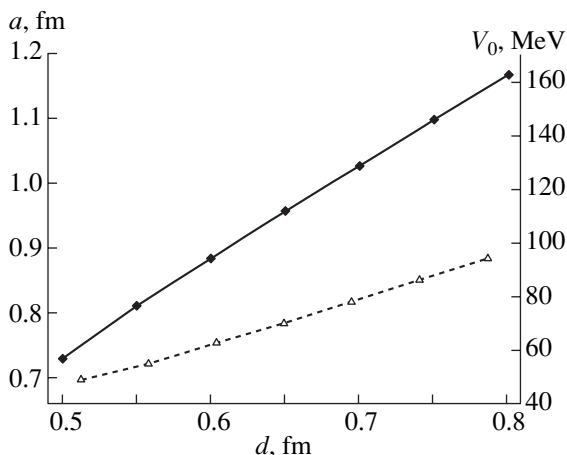


Fig. 7. Diffuseness a (closed diamonds) and depth V_0 (open triangle) of the Woods–Saxon potential versus the diffuseness parameter d of the ground-state nucleon densities for the ^{16}O and ^{208}Pb nuclei.

the nuclei, with the result that the nuclear repulsion between the nuclei, which is due to nuclear-matter compressibility, decreases. This leads to an increase in the depth and width of the capture well.

Figure 6 shows the potential-barrier height $V_{\text{bar}}(d)$ and the potential value at the bottom of the potential well, $V_{\text{well}}(d)$, versus the diffuseness parameter d of the ground-state nucleon densities. With increasing d , the function $V_{\text{bar}}(d)$ decreases linearly, while $V_{\text{well}}(d)$ decreases faster. The capture-well depth, which is determined by the difference $V_{\text{bar}}(d) - V_{\text{well}}(d)$, increases with increasing d .

The HF–BCS approximation describes well the experimental radial density distributions; therefore, the potentials calculated by using the parametrization of the density in the form (15) at the diffuseness-parameter value in the range $d \approx 0.51\text{--}0.6$ fm are

close to realistic potentials at various distances between the nuclei being considered.

4.2. Diffuseness Parameter of the Potential and Cross Section for the Fusion of Nuclei

In order to describe various features of nuclear reactions, the nuclear component of the nucleus–nucleus potential is often parametrized in the Woods–Saxon form [1–3, 7, 28–30, 32–34]

$$V(R) = -V_0 / \{1 + \exp[(R - R_{\text{pot}})/a]\}. \quad (16)$$

For the diffuseness parameter a , it is therefore necessary to determine a value at which the Woods–Saxon potential is close to the realistic potential that was found in the HF–BCS approximation by using Skyrme forces. For this, we will determine the parameters V_0 , R_{pot} , and a in the potential (16) by fitting it to the potential calculated in the ETF approximation at the nucleon-density diffuseness of $d = 0.55$ fm for distances R larger than the sum R_t of the radii of colliding nuclei. After that, the resulting value of R_{pot} is fixed and used in fits to the potential found in the ETF approximation at different values of the diffuseness parameter of the nucleon-density distribution. In this way, we have determined the dependences of a and V_0 on d and plotted them in Fig. 7.

The diffuseness parameter a and the depth V_0 of the Woods–Saxon potential grow almost linearly with increasing diffuseness parameter d of the nucleon densities (see Fig. 7). According to calculations at large distances in the ETF approximation with Skyrme forces, the diffuseness parameter a of the nuclear component of the nucleus–nucleus potential exceeds the diffuseness parameter d of the nucleon distribution in interacting nuclei by a factor of about 1.5.

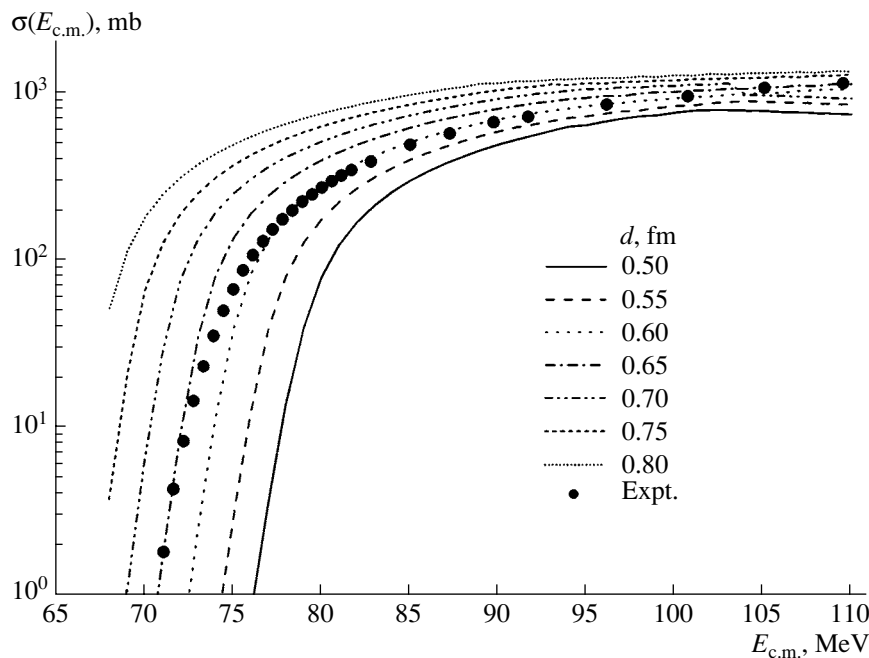


Fig. 9. Cross section for the fusion of ^{16}O and ^{208}Pb nuclei as a function of the c.m. energy for various values of the diffuseness parameter d of the ground-state nucleon densities. The diffuseness parameter of the nuclear potential was set to $a \approx 1.48d$.

As was indicated above, the potential found with the nucleon densities in the form (15) at a nucleon-distribution diffuseness of $d \approx 0.55$ fm corresponds at large distances to the potential obtained with the Hartree–Fock nucleon-density distributions. The corresponding value of the diffuseness parameter of the Woods–Saxon potential is $a \approx 0.81$ fm (see Fig. 7).

Figure 8 shows the result obtained by fitting the Woods–Saxon potential to the nuclear component of the nucleus–nucleus potential calculated in the ETF approximation at the density-distribution diffuseness of $d = 0.55$ fm. At large distances, these potentials agree well with each other, but, in the interior of the nuclei, they are markedly different.

A value of $a \approx 0.81$ fm, which we obtained for the diffuseness parameter of the Woods–Saxon potential, agrees well with that which was proposed earlier. For example, a very close value of $a = 0.788$ fm was found in [8] for the diffuseness parameter of the nucleus–nucleus potential at large distances, while a somewhat smaller diffuseness value of $a = 0.7176$ fm was obtained in [5]. From an analysis of elastic scattering of nuclei, Winther [7] deduced the value of $a = 0.657$ fm. It is very close to the value of $a = 0.65$ fm, which was proposed by Bass in 1980 [1]. On the basis of a systematic investigation of nuclear-fusion reactions, Siwek-Wilczynska and Wilczynski [43] proposed three values of the diffuseness parameter: $a = 0.481$ fm for light, $a = 0.675$ fm for medium-mass, and $a = 0.895$ fm for heavy systems of interacting

nuclei. The analysis of data on the subbarrier fusion of various nuclei in [32–36] led to a rather large diffuseness value in the range $a \approx 0.8–1.5$ fm, the result obtained by studying the subbarrier fusion of ^{16}O and ^{208}Pb nuclei being $a = 1.005$ fm [36].

In the case of interactions of medium-mass and heavy nuclei, diffuseness-parameter values that differ substantially from $a \approx 0.81$ fm are not consistent with realistic nucleon-density distributions in nuclei or with realistic nucleon–nucleon forces. Nevertheless, nucleon-density distributions in light nuclei are characterized by a thin diffuseness layer and are frequently described by a Gaussian function [44]. Therefore, the diffuseness parameter a of the Woods–Saxon potential can assume smaller values in the case of nuclear interactions involving light and very light nuclei. For example, the value of $a = 0.4929$ fm was found in [45] for the diffuseness parameter of the Woods–Saxon potential from an analysis of alpha decay half-lives and cross sections for near-barrier alpha-particle capture by medium-mass and heavy nuclei. An analysis of various reactions induced by $^{12}\text{C} + ^{13}\text{C}$ and $^{12}\text{C} + ^{13}\text{N}$ collisions at near-barrier energies also leads to diffuseness-parameter values substantially smaller than $a \approx 0.81$ fm [46].

In order to study the effect of diffuseness of the potential on the cross section for near-barrier fusion, we will perform calculations for the fusion of ^{16}O and ^{208}Pb nuclei on the basis of the CCFULL code [30].

This code calculates fusion cross sections with allowance for channel coupling to low-lying multipole vibrational surface excitations in both nuclei. In this calculation, the nuclear component of the nucleus–nucleus potential is parametrized in the form of the Woods–Saxon potential (16). The code takes into account nonlinear effects of coupling to multiphonon multipole excitations of the nuclear surface. The parameters of the 2^+ and 3^- excitations are required for calculating the cross sections with the aid of the CCFULL code. They were taken from relevant compilations of experimental data in [47, 48]. The parameters of the nuclear-interaction potential were chosen to be identical to those in Fig. 7. In Fig. 9, the results of the calculations are contrasted against experimental data.

As can be seen from Fig. 9, potentials that were calculated by using small values of the nucleon-density diffuseness parameter d lead to a strong underestimation of the fusion cross section over the entire energy region. As the diffuseness parameter d of the nucleon-density distribution increases, the fusion cross section becomes larger, which is due to the reduction of the fusion-barrier height. However, the slope of the cross section at subbarrier energies is virtually insensitive to variations in d . We note that, here, we did not aim at describing fusion cross sections since our main objective was to reveal the relationship between the diffuseness of the density distribution, the diffuseness of the Woods–Saxon potential, and the fusion cross section.

A comparison of the Woods–Saxon potential with the potential calculated in the ETF approximation (see Fig. 8) and a comparison of fusion cross sections calculated by using the Woods–Saxon potential with relevant experimental data (see Fig. 9) indicate that a realistic nuclear potential is poorly reproduced by the Woods–Saxon form. Both small and large values of the diffuseness parameter of the nucleon-density distributions lead to an inadequate description of experimental data within the CCFULL model. We note that, on the basis of the CCFULL code, one can describe experimental data by simultaneously fitting the parameters V_0 , R_{pot} , and a in (16) (for details, see [36]). However, values found for V_0 , R_{pot} , and a from such a fit do not comply with realistic nucleon-density distributions and realistic nucleon–nucleon forces.

5. CONCLUSIONS

Thus, we have calculated potentials of nucleus–nucleus interaction within Hartree–Fock–Bardeen–Cooper–Schrieffer theory and in the extended Thomas–Fermi approximation, relying on various assumptions on the nucleon-density distributions

in the ground states of the nuclei involved. The potentials were calculated in the frozen-density approximation, which is applicable at collision energies in the barrier region and above. The resulting barrier heights agree well with various approximations proposed previously for nucleus–nucleus interaction. The approximation used to calculate the potentials makes it possible to study in detail various properties of nucleus–nucleus interaction in the vicinity of the point at which colliding nuclei touch each other.

We have shown that a change in the isotopic composition of interacting nuclei affects substantially the height and width of the fission barrier.

The diffuseness parameters of the nucleon-density distributions in nuclei are tightly related to the diffuseness parameter of the potential of nucleus–nucleus interaction. The potential diffuseness parameter a is approximately 1.5 times greater than the diffuseness parameter d of the nucleon-density distribution and is close to 0.81 fm.

Values extracted from experimental data for the diffuseness parameter of the charge-density distribution change from one nucleus to another, lying in the range $d \approx 0.51–0.60$ fm for medium-mass and heavy nuclei (see Table 6.3 in [42]). By virtue of isotopic symmetry, the diffuseness parameters of the neutron-density distribution in medium-mass and heavy spherical nuclei also fall within this interval. Therefore, realistic values of the diffuseness parameter of the potential may lie in the interval $a \approx 0.75–0.90$ fm. In the case of interaction between medium-mass and heavy nuclei, the diffuseness parameter of the potential cannot assume either very small or very large values. It follows that, if values markedly different from those in the range $a \approx 0.75–0.90$ fm are required for describing experimental data within some model, this means that the diffuseness parameters of the nucleon-density distribution and other properties of this distribution do not comply with realistic values or that the proposed model describes inadequately the mechanism of the reaction being considered.

It has been shown that the parametrization of the nuclear component of the nucleus–nucleus interaction in the Woods–Saxon form is unsatisfactory.

REFERENCES

1. R. Bass, *Nuclear Reactions with Heavy Ions* (Springer-Verlag, Berlin, 1980).
2. G. R. Satchler, *Direct Nuclear Reactions* (Clarendon, Oxford, 1983).
3. P. Frobrich and R. Lipperheide, *Theory of Nuclear Reactions* (Clarendon, Oxford, 1996).
4. J. Blocki et al., *Ann. Phys. (N.Y.)* **105**, 427 (1977).
5. W. D. Myers and W. J. Swiatecki, *Phys. Rev. C* **62**, 044610 (2000).

6. H. J. Krappe, J. R. Nix, and A. J. Sierk, *Phys. Rev. C* **20**, 992 (1979).
7. A. Winther, *Nucl. Phys. A* **594**, 203 (1995).
8. V. Yu. Denisov, *Phys. Lett. B* **526**, 315 (2002).
9. V. Yu. Denisov and W. Nörenberg, *Eur. Phys. J. A* **15**, 375 (2002).
10. V. Yu. Denisov, in *Proceedings of the Symposium on Nuclear Clusters: from Light Exotic to Superheavy Nuclei, Rauischholzhausen Castle, Germany, 2002*, Ed. by R. Jolos and W. Scheid (EP Systema, Debrecen, Hungary, 2003), p. 427.
11. V. Yu. Denisov, *AIP Conf. Proc.* **704**, 433 (2004).
12. V. Yu. Denisov and S. Hofmann, *Phys. Rev. C* **61**, 034606 (2000).
13. G. G. Adamian, N. V. Antonenko, and W. Scheid, *Nucl. Phys. A* **678**, 24 (2000).
14. V. I. Zagrebaev, *Phys. Rev. C* **64**, 034606 (2001).
15. Y. Abe, B. Bouriquet, G. Kosenko, and C. Shen, *Nucl. Phys. A* **734**, 168 (2004).
16. W. J. Swiatecki, K. Siwek-Wilczynska, and J. Wilczynski, *Phys. Rev. C* **71**, 014602 (2005).
17. Y. Aritomo and M. Ohta, *Nucl. Phys. A* **753**, 152 (2005).
18. P. Ring and P. Schuck, *The Nuclear Many-Body Problem* (Springer-Verlag, New York, 1980).
19. M. Brack, C. Guet, and H.-B. Hakansson, *Phys. Rep.* **123**, 275 (1985).
20. M. Brack and R. K. Bhaduri, *Semiclassical Physics* (Addison-Wesley, Reading, Mass., 1997).
21. V. M. Strutinski i, A. G. Magner, and V. Yu. Denisov, *Yad. Fiz.* **42**, 1093 (1985) [*Sov. J. Nucl. Phys.* **42**, 690 (1985)]; *Z. Phys. A* **322**, 149 (1985).
22. V. Yu. Denisov and V. A. Nesterov, *Ukr. Fiz. Zh.* **45**, 1164 (2000); *Yad. Fiz.* **65**, 847 (2002) [*Sov. J. Nucl. Phys.* **65**, 814 (2002)].
23. V. A. Nesterov, *Ukr. Fiz. Zh.* **49**, 225 (2004).
24. D. Vautherin and D. M. Brink, *Phys. Rev. C* **5**, 626 (1972).
25. J. Dobaczewski, H. Flocard, and J. Treiner, *Nucl. Phys. A* **422**, 103 (1984).
26. S. A. Fayans et al. *Nucl. Phys. A* **676**, 49 (2000).
27. J. W. Negele, *Rev. Mod. Phys.* **54**, 913 (1982).
28. M. Dasgupta, D. J. Hinde, N. Rowley, et al., *Annu. Rev. Nucl. Part. Sci.* **48**, 401 (1998).
29. A. B. Balantekin and N. Takigawa, *Rev. Mod. Phys.* **70**, 77 (1998).
30. K. Hagino, N. Rowley, and A. T. Kruppa, *Comput. Phys. Commun.* **123**, 143 (1999).
31. V. Yu. Denisov, *Yad. Fiz.* **62**, 1431 (1999) [*Phys. At. Nucl.* **62**, 1349 (1999)]; *Eur. Phys. J. A* **7**, 87 (2000).
32. K. Hagino, N. Rowley, and M. Dasgupta, *Phys. Rev. C* **67**, 054603 (2003).
33. D. J. Hinde, A. C. Berriman, R. D. Butt, et al., *Eur. Phys. J. A* **13**, 149 (2002).
34. M. Dasgupta and D. J. Hinde, *Nucl. Phys. A* **734**, 148 (2004).
35. J. O. Newton, R. D. Butt, M. Dasgupta, et al., *Phys. Rev. C* **70**, 024605 (2004).
36. C. R. Morton, A. C. Berriman, M. Dasgupta, et al., *Phys. Rev. C* **60**, 044608 (1999).
37. H. De Vries, C. W. De Jager, and C. De Vries, *At. Data Nucl. Data Tables* **36**, 495 (1987).
38. K. A. Brueckner, J. B. Buchler, and M. M. Kelly, *Phys. Rev.* **173**, 944 (1968).
39. G. Bertsch, *Z. Phys. A* **289**, 103 (1978).
40. J. F. Liang, D. Shapira, C. J. Gross, et al., *Phys. Rev. Lett.* **91**, 152701 (2003).
41. S. Hofmann and G. Münzenberg, *Rev. Mod. Phys.* **72**, 733 (2000).
42. R. C. Barrett and D. F. Jackson, *Nuclear Sizes and Structure* (Clarendon, Oxford, 1977; Naukova Dumka, Kiev, 1981).
43. K. Siwek-Wilczynska and J. Wilczynski, *Phys. Rev. C* **69**, 024611 (2004).
44. I. Tanihata, D. Hirata, T. Kobayashi, et al., *Phys. Lett. B* **289**, 261 (1992).
45. V. Yu. Denisov and H. Ikezoe, *Phys. Rev. C* **72**, 064613 (2005).
46. B. Imanishi, V. Denisov, and T. Motobayashi, *Phys. Rev. C* **55**, 1946 (1997).
47. S. Raman, C. W. Nestor, and P. Tikkanen, *At. Data Nucl. Data Tables* **78**, 1 (2001).
48. T. Kibedi and R. H. Spear, *At. Data Nucl. Data Tables* **80**, 35 (2002).

Translated by A. Isaakyan